Chemical Physics 102 (1986) 349–363
North-Holland, Amsterdam

ANALYSIS OF THE CHEMILUMINESCENCE FROM ELECTRONICALLY EXCITED LEAD OXIDE GENERATED IN A FLOW TUBE REACTOR

E.A. DORKO, J.W. GLESSNER, C.M. RITCHEY, L.L. RUTGER, J.J. POW, L.D. BRASURE, J.P. DURAY and S.R. SNYDER

Department of Engineering Physics, Air Force Institute of Technology, Wright–Patterson AFB, OH 45433-6583, USA

Received 10 May 1985; in final form 10 October 1985

The chemiluminescence from electronically excited lead oxide formed during the reaction between lead vapor and either $^3\Sigma$ O_2 or $^1\Delta$ O_2 has been studied. The reactions were accomplished in a flow tube reactor. A microwave discharge was used to generate $^1\Delta$ O_2. The vibronic spectrum was analyzed and the band head assignments were used in a linear least-squares calculation to obtain the vibronic molecular constants for the X, a, b, A, B, C, C′, D, and E electronic states of lead oxide. Based on these and other molecular constants, Franck–Condon factors were calculated for the transitions to the ground state and also for the A–a and D–a transitions. Evidence was presented to support a kinetic analysis of the mechanism leading to chemiluminescence under the experimental conditions encountered in the flow tube reactor. Mechanisms presented earlier were verified by the present data.

1. Introduction

The lead oxide molecule (PbO) has been extensively studied since the early 1900's. To observe the band spectra, early researchers used lead chloride gas flames or lead chloride carbon arcs. Subsequently, high-resolution absorption and emission studies identified at least six band systems, all of which terminated on the ground state [1,2].

More recently, using a molecular beam system, Oldenborg et al. [2] were able to perform emission spectroscopy and laser-induced fluorescence studies of the PbO system. By reacting atomic lead with O_3 under single collision conditions, they identified a series of 55 bands in the region 450–850 nm assigned to transitions from the a and b states. Their analysis showed that all bands were emissions to the ground state from excited electronic states. They postulated the following mechanism to be responsible for the population of the electronically excited a state of lead oxide (PbO*)

$$\mathrm{Pb(S)} \xrightarrow{\text{heat}} \mathrm{Pb}(^3\mathrm{P}_0), \tag{1}$$

$$\mathrm{Pb}(^3\mathrm{P}_0) + \mathrm{O}_3 \rightarrow \mathrm{PbO}^*(\mathrm{a}) + \mathrm{O}_2. \tag{2}$$

They studied the chemiluminescent intensity of this reaction as a function of oven temperature (T) under the single collision conditions of their molecular beam system. By plotting the logarithm of the intensity versus $1/T$, they were able to find the activation energy. They concluded that (i) the chemiluminescence was first order in Pb, with no dependence on other components such as Pb_2, and that (ii) the reaction activation energy was small.

They also observed unusual variations in chemiluminescent intensities of the B–X transition with changes in oven temperature. They found that the intensity decreased with increasing oven temperature over certain temperature ranges. They attributed this phenomenon to a discharge near the oven which was exciting some Pb atoms to the metastable $^3P_1$ or $^3P_2$ levels presumably giving rise to metastable population densities greater than expected from a Boltzmann distribution. The reaction of these excited Pb atoms with O_3 produced the B–X chemiluminescent feature.

Kurylo et al. [3] also studied the reaction of lead and ozone. Their studies were accomplished in a flow tube reactor in which multiple collisions were possible. They observed emissions from the a,

b, A, and B states. Using laser excitation of the O_3, they recorded a significant increase in A state emission intensity over the a, b, and B states. They have postulated two mechanisms for the enhancement. First, as a result of laser excitation of O_3, the reaction with $Pb(J = 1)$ produces PbO^* in the B state in higher vibrational energy levels. This energy is then collisionally transferred to another molecule which is excited to the A state. Another possibility is that the vibrational energy in the excited O_3 directly increases the rate of A state production at the expense of other reaction channels. Their observation of chemiluminescence over several feet in their flow system indicates that a slow reaction with $Pb(J = 0)$ must compete favorably with a fast reaction with $Pb(J = 1)$.

Linton and Broida [4] investigated the reactions of lead with N_2O, O, O_2, and O_3 by studying the spectra of the chemiluminescence from electronically excited PbO generated in a flow tube system under a wide variety of conditions. They found that spectral intensities were very dependent on the oxidizer used and on the oxidizer pressure. They tabulated eight band systems between 250 and 800 nm and observed 22 new bands in the PbO system.

Brom and Beattie [5] used a flash-lamp-pumped tunable dye laser to study the a–X band system of PbO. They were able to obtain high-resolution spectra which allowed calculation of rotational constants. Observation of P, Q, and R rotational branches confirmed that Hund's case c is the angular momentum coupling scheme for the a state of PbO.

Wicke et al. [6] studied the velocity dependence of the $Pb + N_2O \rightarrow PbO(B, v = 0) + N_2$ chemiluminescence reaction under single collision conditions in an atomic beam. They were able to show that the chemiluminescence due to the B–X transition was a function of the translational energy of the reactant Pb atoms.

The most recent work with PbO was reported by Bachar and Rosenwaks [7]. While studying the reaction of Pb with $^1\Delta$ O_2, they observed emissions from the a, b, A, B, C, C′, and D states. Using microwave and chemical sources of $^1\Delta$ O_2, they were able to compare the effects of $^1\Delta$ O_2 concentration on the relative intensities of the various states. In going from 10% concentration to 30%, they noted a significant increase in intensity from all the states with the enhancement of the high energy D state about twice that of the other states.

They also studied the kinetic mechanism of the reaction by taking into account the concentration of excited species and exothermicity of possible reactions. Based on their results they concluded that, for the case of the $Pb + {}^1\Delta$ O_2 reaction, the main source of $Pb(^3P_1)$ was a reaction between $O_2(^1\Delta)$ and $Pb(^3P_0)$ [7].

In the present work, we report on the results obtained when lead vapor was reacted with either ground state molecular oxygen ($^3\Sigma$ O_2) or with the electronically excited state ($^1\Delta$ O_2) in a flow tube reactor. Some preliminary results have been reported on a portion of this work [8]. In the present account we report on the complete spectroscopic analysis of the vibronic transitions from the a, b, A, B, C, C′, D, and E states to the ground state of PbO.

In section 2 the experimental and computational techniques are described. Section 3 contains the results of the vibronic band head assignments, molecular constants based on the assignments, and Franck–Condon factors for the transitions.

In section 4 the experimental evidence which has a bearing on determining the mechanisms responsible for the chemiluminescence is discussed. A comparison is made between the mechanisms for formation of PbO^* during the reaction between Pb and $^3\Sigma$ O_2 and Pb and $^1\Delta$ O_2.

2. Experimental and computational procedures

2.1. Flow tube reactor

The experimental apparatus used to generate the chemiluminescent PbO flame was a flow tube reactor. The reactor has been described in detail previously [8]. For the reactions between Pb and $^3\Sigma$ O_2 a stainless-steel oxidizer manifold was used as described previously [8]. For the work with $^1\Delta$ O_2 the stainless-steel oxidizer manifold was replaced by one made of pyrex glass. Pyrex was used because of its very low quenching coefficient for $^1\Delta$ O_2 (10–5) [7]. The manifold consisted of a section

of 14 mm i.d. pyrex tubing flared at one end. A series of six rows of four holes each were drilled in the tubing. The holes were 0.8 mm in diameter and were drilled with a diamond impregnated bit. The first row of holes was drilled in the flared edge at a 45 degree angle to the tube proper. The rows were spaced 3 mm apart, and each row was offset from the previous row by 45 degree to prevent stress fractures during drilling. Once the holes were drilled, a section of 28 mm o.d. tubing was placed over the smaller tubing, and the two sections were sealed together. This formed a double-walled cylinder with an open center. Finally, the pyrex stem was attached to the lower edge of the cylinder.

The manifold was mounted over the chimney. The stem of the pyrex manifold was secured to the flow tube via a 1/2 in. Cajon connector welded on a stainless-steel plate. The plate was attached to one of the side ports of the cross. Due to the fragility of the manifold, extreme care was taken when installing or removing the manifold.

Spectra were obtained as described previously [8]. Resolution of spectral lines with the experimental arrangement was determined to be 5 Å fwhm.

2.2. Generation of $^1\Delta$ O_2

The $^1\Delta$ O_2 was generated using a 2450 MHz microwave discharge cavity. Pure O_2 was passed through a 13 mm quartz tube which was surrounded by a McCarroll-type microwave cavity (Opthos instruments) [9]. The cavity was cooled with an air stream directed into the cavity in order to stabilize the discharge. The quartz tube was connected by a means of pyrex tubing to the oxidizer manifold. A yellow brown coating of HgO was deposited on the pyrex tubing downstream of the cavity to significantly reduce any atomic oxygen which may have formed in the discharge [10].

2.3. Emission intensity measurements

Intensities of emissions at selected wavelengths were observed under different pressure conditions as described previously [8]. The intensities were observed as a function of lead vapor temperatures. From these observations a rough estimate of the activation energies (E_a) for the formation of PbO* with both $^3\Sigma$ O_2 and 1Δ O_2 were obtained [2]. The results of these experiments are presented in table 1.

2.4. Determination of the presence and concentrations of electronic states of Pb

Previously [8] it had been shown that only a thermal mechanism was operating to produce lead vapor. An experimental determination of the number densities of thermally excited Pb was precluded due to a lack of necessary detection equipment. However, from a knowledge of the oven temperature and the energies of the states of Pb, the relative concentrations of the electronically excited states can be calculated using the Boltzmann equation. The energy levels or the first five states of Pb are shown in table 2. The relative number densities $N_{^3P_1}$ and $N_{^3P_2}$ were found to be 6.3×10^{-5} and 1.9×10^{-6}, respectively at a crucible temperature of 1163 K. The concentration of Pb in the flame region was shown to be $\approx 3.4 \times 10^{14}$ atoms/cc [8]. Assuming for the moment that

Table 1
Activation energies for the formation of PbO *

Wavelength observed (nm)	O_2 pressure (Torr)	Ar pressure (Torr)	Pb vapor temperature (K)	Activation energy (E_a) (kcal/mol)
Pb + $^3\Sigma$ O_2				
670, 590.8	0.3	1.9	1044–1086	63.9 ± 8.0
590.8, 431.3	0.8	3.3	1062–1103	115.3 ± 22.4
Pb + $^1\Delta$ O_2				
590.8, 431.3	0.7–1.3	0.9–1.0	809–1048	21.0 ± 6.1

Table 2
Energy levels of Pb [11]

State	Energy (cm^{-1})
$^3P_0$	0
$^3P_1$	7819
$^3P_2$	10650
$^1D_2$	21457
$^1S_0$	29466

all excited species created in the crucible reach the flame region, this would yield approximate concentrations of 2.1×10^{10} atoms/cc for $Pb(^3P_1)$ and 6.5×10^8 atoms/cc for $Pb(^3P_2)$. Concentrations of $Pb(^1D_2)$ and $Pb(^1S_0)$ were negligible.

The relative ratios of the excited state population were calculated at the crucible temperature. To verify that this ratio remains constant into the flame region the following analysis was performed.

Transitions between the five lowest energy states of Pb are prohibited due to Laporte's rule which indicates that transitions between states of the same parity are forbidden [12,13]. Thus, the first four excited states of Pb are metastable.

The transition probabilities for transitions between the three lower states of Pb have been reported by Garstang [14] and are tabulated in table 3. A_m is the magnetic dipole transition probability and A_q is the electric quadrupole transition probability. Based on these values, the lifetime of the $^3P_1$ and $^3P_2$ states can be calculated from

$$\tau = 1/p, \tag{3}$$

where p is the probability of a transition. This yields a lifetime of 136 ms for the $^3P_1$ state. Since the probabilities are additive for a given state [14], the lifetime of the $^3P_2$ state is 4.8 s. For the current system, the Pb flow velocity was calculated to be 8150 cm/s [8]. Since the chimney of the flow tube is 4 in. long, the residence time of the Pb in the chimney is ≈ 1.25 ms. Therefore, any $^3P_1$ and $^3P_2$ formed in the crucible will reach the flame region unless quenched by collisions with Ar molecules or the chimney walls.

Table 3
Transition probabilities between excited states of Pb [14]

Transition	Type	Probability (s^{-1})
$^3P_2-^3P_1$	A_m	0.18
	A_q	2.5×10^{-4}
$^3P_2-^3P_0$	A_q	0.21
$^3P_1-^3P_0$	A_m	7.30

The equation for the change in $Pb(^3P_1)$ concentration due to collisions with Ar can be written as

$$d[Pb(^3P_1)]/dt = k'_{Ar}[Pb(^3P_1)], \tag{4}$$

where [ ] indicates concentration and k'_{Ar} is a first-order collision rate constant. The constant k'_{Ar} is defined in terms of a second-order rate constant, k, and the concentration of Ar as

$$k'_{Ar} = k[Ar]. \tag{5}$$

Hussain and Littler [15] reported a value for k of 0×10^{-16} cc/molecule s at 300 K with estimated error limits of $\pm 1.0 \times 10^{-16}$. The temperature extremes in the flow tube ranged from 300 to 1163 K and correspond to the greatest and least concentrations of Ar, respectively. Applying the ideal gas equation of state to both temperatures at an Ar pressure of 2 Torr yields the following Ar concentrations:

$$[Ar]_{300\,K} = 6.439 \times 10^{16} \text{ molecules/cc}, \tag{6}$$

$$[Ar]_{1163\,K} = 1.656 \times 10^{16} \text{ molecules/cc}. \tag{7}$$

These concentrations were substituted into eq. (5) using the largest value for k (1×10^{-16}) and resulted in the following rate constants for de-excitation:

$$k'_{300\,K} = 6.439 \text{ s}^{-1}, \tag{8}$$

$$k'_{1163\,K} = 1.656 \text{ s}^{-1}. \tag{9}$$

Upon taking the inverse of these rate constants, the following lifetimes are obtained:

$$\tau_{300\,K} = 155 \text{ ms}, \tag{10}$$

$$\tau_{1163\,K} = 603 \text{ ms}. \tag{11}$$

A similar analysis for the $^3P_2$ state using $k = (2.0$

$\pm 0.5) \times 10^{-15}$ cc/molecule s resulted in the following lifetimes

$$\tau_{300\,K} = 6 \text{ ms}, \quad (12)$$

$$\tau_{1163\,K} = 20 \text{ ms}. \quad (13)$$

As seen from these results, even in the worst case, the lifetimes of the $^3P_1$ and $^3P_2$ states are at least four times greater than the chimney residence time of lead.

Since this analysis has neglected the effects of collisions with the chimney walls, these calculations represent an upper limit on the lifetimes. However, the effect of wall collisions is assumed to be negligible. Thus, any $^3P_1$ or $^3P_2$ created in the crucible will reach the flame region.

Bachar and Rosenwaks have previously observed the presence of atomic lead vapor in the ground and electronically excited states [7]. In the present work, evidence was gathered for the presence of atomic lead species in the flame region. The fluorescence of the lead/argon gas stream was observed. The excitation source was a lead iodide electrodeless lamp [16]. Excitation was provided by a microwave cavity operating at 2450 MHz. Emission from the Pb/Ar stream was observed at right angles to the incident light path. Under these conditions, two weak fluorescence lines were observed which are attributable to atomic lead – one at ≈ 4055 Å and another broad emission in the region of 3600 Å.

Wood and Andrew [17] have studied the emission from neutral lead in a lead halide electrodeless discharge tube. In their report they used the term symbols suggested in ref. [18] to identify the energy states for atomic lead which was assumed to obey *jj* coupling. They assigned the two most intense emission lines in the spectrum (with a ratio of intensities of 9 : 5) to the transition $6p7s(1/2, 1/2)_1 \rightarrow 6p^2(3/2, 1/2)_2$ at 4057.8067 Å and $6p7s(1/2, 1/2)_0 \rightarrow 6p^2(3/2, 1/2)_1$ at 3639.5677 Å, respectively. Assuming *LS* coupling, the transitions are designated as $6p7s(^3P_1) \rightarrow 6p^2(^3P_2)$ and $6p7s(^3P_0) \rightarrow 6p^2(^3P_1)$, respectively.

In the present study it is reasonable to assume that excitation of the $6p^2(^3P_2)$ and $6p^2(^3P_1)$ states of Pb in the flow tube occurred under the influence of these two emission lines from the PbI lamp. The fluorescence observed was simply the reverse of the excitation process. This evidence indicates that the two lowest lying, electronically excited states of Pb did exist in the Pb/Ar gas stream in the flame region of the flow tube prior to any energy exchange due to collisions with oxidizer or product particles.

Wood and Andrew [17] report that a strong transition to the $6p^2(^3P_0)$ state of Pb [i.e. $6p7s(1/2, 1/2)_1 \rightarrow 6p^2(1/2, 1/2)_0$] occurs at 2833.0534 Å with ≈ 11% of the intensity of the most intense emission line. Under the conditions of our experiment this transition from the $^3P_0$ state could not be observed since a glass sleeve surrounding the PbI lamp absorbed radiation in the UV spectral region. However, if the excited states are present, then the ground state must also be present in the Pb/Ar gas stream under the experimental conditions. That is, since the lead was vaporized under exclusively thermolytic conditions, it is reasonable to assume that the number densities of the three electronic states are at least roughly estimated by a Boltzmann distribution which predicts a preponderance of the lowest energy state.

2.5. Computational procedures

Molecular constants were calculated by means of a global least-squares computer program, Program DUNAM [19], written by D.G. Shankland. The program was written in FORTRAN 77 to be used on a Harris 500 computer. Computation time for the analysis was typically a few seconds. The program uses as input the wavelength of the transition, the assignment, and a weighting factor (if desired). The program calculates molecular constants for all of the energy states involved in the vibronic transitions.

Franck–Condon factors were calculated from the molecular constants by use of program FCFACT written by J.J. Pow and L.D. Brasure [18]. The program FCFACT was written in FORTRAN 5 for use on a CDC Cyber computer. Values for the wavefunctions used in the calculations were obtained by use of program RIPA provided by C.R. Vidal of the Max-Planck Institute for Extraterrestrische Physik, FRG [21–23].

This program uses the semiclassical RKR approach to calculate an initial potential energy curve for a diatomic molecule [24–26] starting with molecular constants calculated from spectroscopic data. It then uses this calculated potential in a quantum-mechanical calculation developed initially by Hinze and Kosman [27] known as the inverted perturbation approach (IPA). This calculation refines the potential and produces numerical values for the wavefunctions. These values for the wavefunctions are then used to calculate the Franck–Condon factors for the vibronic transitions.

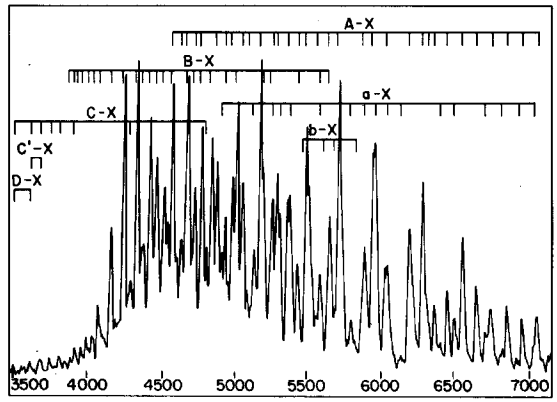

Fig. 1. Chemiluminescence spectrum from the reaction between lead vapor and $^1\Delta$ O_2.

3. Results

3.1. Vibronic band head assignments and molecular constants

The chemiluminescence of PbO was observed during the reaction between Pb and $^3\Sigma$ O_2 and $^1\Delta$ O_2. In both cases the emissions were sufficiently intense so that the spectral lines could be resolved. Spectra were observed from 300 to 900 nm. The vibrational band structure was observed in all spectra with the rotational structure being shaded toward the red. The rotational structure could not be resolved; however, band head assignments could be made with a good degree of certainty in many cases. The slit width for spectra of the Pb + $^3\Sigma$ O_2 reaction was 150 μm, and the slit width for spectra of the Pb + $^1\Delta$ O_2 reaction was 15 μm. A low-dispersion spectrum obtained during the reaction between Pb and $^1\Delta$ O_2 is shown in fig. 1. Band head assignments for the chemiluminescence spectrum from Pb + $^3\Sigma$ O_2 have been reported previously [8]. Analysis of the spectrum allowed identification of 63 vibronic bands assignable to transitions from the a, A, B, and C electronic states. Analysis of the spectrum from Pb + $^1\Delta$ O_2 allowed identification of 271 vibronic bands assignable to transitions from the a, b, A, B, C, C′, D, and E electronic states [19,28]. Based on these assignments the vibronic molecular constants for eight energy states of PbO have been calculated using program DUNHAM [19]. The constants are listed in table 4. For comparison, the molecular constants reported previously are listed in table 5. It is noted that there is a large variation in the reported values of the constants. The constants reported by Oldenborg et al. [2] for the X and a states appear to be the most reliable. Likewise the values reported by Linton and Broida [4] for the A state appear to be the most reliable. The constants calculated in the present work agree to within 1 or 2 standard deviations with those reported by Oldenborg et al. for the X and a states and within 2 or 3 standard deviations within those reported by Linton and Broida for the A state. Discrepancies between the sets of values for the constants may be due to the method used to weight the data during the calculations. Both previous reports [2,4] used a weighting technique in their least-squares

Table 4
Molecular constants for PbO in cm^{-1}. (Numbers in parentheses are two standard deviations)

Electronic state	T_e	$\bar{\omega}_e$	$\bar{\omega}_e x_e$
X	0	722.69(0.96)	3.613(0.060)
a	16031.1(8.0)	483.4(3.0)	2.71(0.24)
b	16335.4(12.8)	433.5(10.6)	−0.04(1.80)
A	19876.2(6.6)	445.2(3.0)	0.78(0.30)
B	22303.6(8.0)	491.7(4.0)	0.98(0.42)
C	23794.6(11.2)	550.6(4.6)	5.46(0.38)
C′	24941.9(11.8)	500.1(4.2)	3.40(0.30)
D	30059.3(13.8)	617.7(10.0	9.56(1.60)
E	34443.0(22.4)	477.4(25.6)	13.0(5.2)

Table 5
Previously reported molecular constants for PbO in cm^{-1}. (Numbers in parentheses are two standard deviations)

State	T_e	$\bar{\omega}_e$	$\bar{\omega}_e x_e$	Ref. (year)
X	–	720.97(0.72) [a]	3.536(0.050) [a]	[4] (1976)
	–	722.9(2.8) [a]	3.766(0.4) [a]	[2] (1975)
	–	721.26	3.53	[29] (1970)
	–	721.6	3.70	[30] (1961)
	–	722.3	3.73	[1] (1930)
a	16024.9(2.9) [a]	481.5(1.4) [a]	2.45(0.14) [a]	[4] (1976)
	15912 [b]	478.4 [b]	2.5 [b]	[3] (1976)
	16029(8) [a]	478.7(1.9) [a]	2.292(0.128) [a]	[2] (1975)
b	16315 [b]	441.0 [b]	–	[3] (1976)
	16379 ± 430	–	–	[2] (1975)
A	19862.6(3.0) [a]	444.3(1.6) [a]	0.54(0.24) [a]	[4] (1976)
	19721 [b]	441.9 [b]	0.20 [b]	[3] (1976)
	19862.3	444.2	0.46	[30] (1961)
B	22166 [b]	502.0 [b]	3.8 [b]	[3] (1976)
	22289	489	–	[30] (1961)
	22289.8	496.3	2.33	[1] (1930)
C	23820	532	3.9	[29] (1970)
C′	24947	494	3.0	[29] (1970)
D	30194	530.4	2.9	[29] (1970)
	30197.0	530.6	1.05	[1] (1930)
E	34455	454.1	6.95	[29] (1970)

[a] Calculated by a weighted least-squares technique.
[b] Calculated based on ground state constants of ref. [29].

calculations. In the present work no weighting was used. However, the agreement is still within acceptable error limits between the different values. For the states other than the X, a, and A state no statistical estimates of reliability have been placed on the values for the constants. The values presented in this work can be accepted as useful constants within the reliability limits placed on them. It is to be noted that these limits are rather large for the E state constants. The number of identified bands in the E–X transition was only seven. This limited data set has lead to a relatively large standard deviation for the E state constant.

3.2. Franck–Condon factors

Franck–Condon factors were calculated for transitions from each of the electronic excited states to the ground state. In addition, factors for the D–a and A–a transition have been calculated. The vibronic constants listed in table 4 were used for the calculations. Rotational constants and dissociation energies were obtained from the data listed by Huber and Herzberg [31].

In order to calculate Franck–Condon factors, the numerical values of the wavefunctions need to be known. Using program RIPA, the values of the wavefunctions for the vibrational levels of each electronic state were calculated for a total of 25 levels (beginning at $v = 0$) and evaluated at 301 points on each vibrational level. It was important to stay within the accurate portion of the potential energy curve when extending the number of levels calculated [32]. The pure reflection approximation begins to break down near the dissociation energy and special procedures need to be undertaken to maintain the desired level of accuracy in this region. For all states of PbO except the E state, level 24 is within the reliable region. The E state has the highest potential energy of the PbO excited states observed in emission and is very wide and shallow. The state is difficult to calculate and the maximum vibrational level accurately attainable is 15. Because of the overlap between the E and X states and because of the requirements of the program

FCFACT, a minimum of 351 points were required to give a valid calculation of the Franck–Condon factors for the transitions between these two states. The Franck–Condon factors for the a–X, A–X, B–X, and A–a transitions are shown in the appendix. Other values are available upon request [20].

Comparison of these Franck–Condon factors with a few that had been calculated previously and reported by Suchard [33] shows a good (though not exact) correspondence between the values. The lack of complete correspondence is due to the use of different molecular constants in the different sets of calculations.

4. Discussion of the mechanisms which lead to the observed chemiluminescence from the PbO*

4.1. Chemiluminescence during the reaction between lead and $^3\Sigma$ O_2

A mechanism to account for the formation of PbO* during the reaction between Pb and $^3\Sigma$ O_2 has been presented previously [8]. At higher pressure the following two-step mechanism:

$$\mathrm{Pb(g)} + \mathrm{O_2}(^3\Sigma) \rightarrow \mathrm{PbO(X)} + \mathrm{O}(^3\mathrm{P_2}), \qquad (14a)$$

$$\mathrm{Pb(g)} + \mathrm{O}(^3\mathrm{P_2}) + \mathrm{M} \rightarrow \mathrm{PbO^*} + \mathrm{M}, \qquad (14b)$$

is postulated to account for the data. (Eq. (14b) may very well be a termolecular reaction involving an energy sink species, M.) At lower pressure, on the other hand, Pb flow rates are slower and there is time for the atomic lead to condense to molecular lead in the flame region of the flow tube. In this pressure regime the four-center mechanism

$$\mathrm{Pb_2(g)} + \mathrm{O_2}(^3\Sigma) \rightarrow \begin{array}{c}\mathrm{Pb} \cdots \mathrm{Pb} \\ \vdots \quad\quad \vdots \\ \mathrm{O} \cdots \mathrm{O}\end{array} \rightarrow \mathrm{PbO^*} + \mathrm{PbO}, \qquad (15)$$

accounts for the data. The evidence presented in section 2 shows the presence of electronically excited species of Pb, that is the $^3P_1$ and $^3P_2$ states, in addition to the presence of the $^3P_0$ ground state. Since reaction (14a) is the slow or rate-controlling step in the reaction between atomic lead and $^3\Sigma$ O_2, this reaction pathway is expected to be slow compared to the pathway shown in (15) which has a much lower activation energy. However, if the concentration of Pb_2 is low compared to the concentration of atomic Pb then both reactions can occur at comparable rates. Evidence for the existense of Pb_2 under conditions similar to the present experiment has been presented by Johnson [34]. He observed and characterized the laser-induced fluorescence from a lead species carried in a stream of inert gas from a resistively heated alumina crucible through a fluorescence cell. The fluorescing species was identified as Pb_2. Since both Pb and Pb_2 are present under the experimental conditions in the flow tube, both mechanisms can occur. Slight variations in experimental conditions can lead to a change in the relative rates of formation of PbO* by the two mechanisms. Since the exothermicities of the two mechanisms are different, the relative amounts of the excited PbO* species which form should vary with experimental conditions. This variation in relative intensity with oxidizer pressure had been observed primarily during the reaction of lead with other oxidizers by Linton and Broida [4].

In the present work an analysis similar to that performed by Linton and Broida was performed. Five spectral determinations were made in the region 350–870 nm. In all five spectra the argon carrier gas pressure was kept constant at 2.1 Torr. The five oxidizer pressures were 0.04, 0.1, 0.2, 0.4, and 0.7 Torr. From these spectra it was apparent that as the O_2 pressure was increased from 0.04 to 0.2 Torr there was a gradual increase in the emission intensity from the a, A, and B states. At 0.4 Torr however, there was a dramatic increase in emission from the B and A states relative to the a state. Then, at 0.7 Torr, the strong enhancement of the B and A state had subsided and the spectra more closely resembled that observed at 0.1 and 0.2 Torr. Fig. 2 shows a plot of the log of the ratio of the emission intensity of different lines at 0.4 Torr to the intensity observed at 0.1 Torr versus energy above the ground state. Line enhancements in the a state are relatively small with enhancement factors of 1.1–1.2 and some lines are even inhibited. Enhancement factors for the A state are

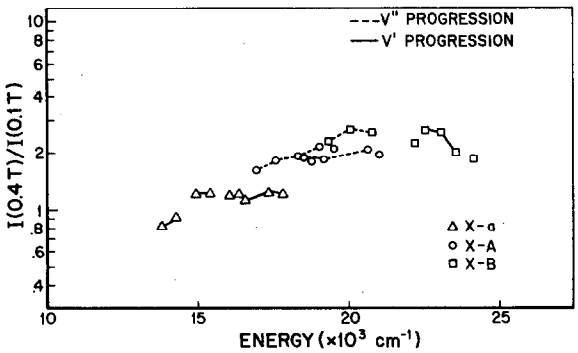

Fig. 2. Plot of the log of the ratio of the intensity at 0.4 Torr oxidizer pressure to the intensity at 0.1 Torr versus energy of the emitted photon for the reaction between lead vapor and $^3\Sigma$ O_2.

between 1.6 and 2.2. The strongest enhancement occurs in emission from the B state. Here factors range from 1.87 to 2.7. The general trend of the data is similar to Linton and Broida's results observed in the Pb + O_3 reaction; (6% O_3 in O_2) [4]. The pressures involved are also similar. This suggests that much of the emission observed by Linton and Broida was actually due to the Pb + O_2 reaction. Also, the chemistry of the two reactions may be quite similar. Indeed, after the initial reaction with O_3, the chemistry may proceed along the same lines.

A gradual increase or decrease in emission intensity from the excited states as pressure is varied is not unexpected. Indeed, the intensity should reach a maximum at a point corresponding to the most efficient mixing of O_2 and lead vapor. However, this does not explain why some states are enhanced more than others. The explanation for this observation is that two (or more) mechanisms are operating to produce PbO*. While the reaction with atomic lead can produce PbO* in the E state this reaction is relatively slow compared to the reaction with Pb_2 which can produce PbO* only up to the A state with ground state Pb_2 or up as high as the B state with excited Pb_2. The relative rates at which the two mechanisms occur, account for the changes in the relative intensities.

Table 6
Intensity ratios for the a–X, A–X and B–X transitions [a)]

Transition	I_2/I_1	Transition	I_2/I_1
a(1,3)	6	A(0,1)	192
a(1,2)	5	A(2,1)	329
a(2,2)	15	A(1,0)	153
a(1,1)	8	A(3,1)	180
a(2,1)	7	A(2,0)	296
a(1,0)	8	A(3,0)	176
a(3,1)	17	A(4,0)	238
a(2,0)	28	B(0,3)	65
a(4,1)	33	B(0,2)	81
a(3,0)	16	B(1,2)	86
a(4,0)	27	B(0,1)	53
a(5,0)	37	B(1,1)	131
A(0,4)	135	B(1,0)	106
A(1,4)	67	B(2,0)	160
A(0,3)	116	B(3,0)	238
A(1,3)	36	B(4,0)	276
A(0,2)	70	B(5,0)	129
A(1,2)	173		

[a)] I_1 is the intensity of the chemiluminescence observed during the reaction between lead and $^3\Sigma$ O_2; I_2 is the intensity observed during the reaction between lead and $^1\Delta$ O_2.

4.2. Chemiluminescence during the reaction between lead and $^1\Delta$ O_2

The low dispersion spectrum shown in fig. 1 obtained during the reaction between lead and $^1\Delta$ O_2 showed a gain ≈ 100 times greater than that obtained during a similar experiment with lead and $^3\Sigma$ O_2 [8]. The value of 100 was calculated from differences by factors of 10 in the slit width and in the carrier gas pressure (Pb flow rate). These spectra allow a qualitative comparison of the relative intensities of the different electronic systems. Taking into account the differences in gain, the Pb + $^1\Delta$ O_2 reaction obviously caused a considerable increase in the intensity of emissions from all of the excited states. However, the A and B state emission intensities were increased much more than the a state emission intensities. The ratios of intensities for several representative transitions are shown in table 6.

Based on these figures and after taking an average ratio for each state, the enhancement of the A state was calculated to be ≈ 10 times that for the a state. Similarly, the enhancement of the B state was ≈ 8.3 times that for the a state. These enhancements of the A and B states over the a

state offer additional evidence that it may be possible to populate an upper electronic energy state at the expense of a lower-lying energy state [4,7]. If this upper state population could achieve greater than 50% of the lower-lying energy state, a population inversion would be accomplished.

Total O_2 pressures were varied from 0.3 to 0.9 Torr at 0.5 Torr of Ar and from 1.0 to 1.4 Torr at 0.9 Torr of Ar. (No attempt was made to monitor changes in $^1\Delta$ O_2 production with changes in total O_2 pressure.) A slight enhancement of the B state emission intensity over that of the a state was noted when the total O_2 pressure was increased from 0.3 to 0.7 Torr. However, this enhancement subsided at 0.8 Torr and was not observed at higher pressures. The major relative enhancements (i.e. factors of up to 2.7) of the A and B state emissions observed for the reaction of Pb + $^3\Sigma$ O_2 with increases in oxidizer pressures was not observed for the Pb + $^1\Delta$ O_2 reaction. The present results are consistent with the much more quantitative experiments of Bachar and Rosenwaks [7]. They did not observe significant increases in emission intensities from the A and B states relative to those from the a state with an increase in $^1\Delta$ O_2 pressure. They did observe increases in intensities from C and D state emission transitions relative to a state emission transitions by a factor of approximately two. These relative intensity increases were less than those observed when $^3\Sigma$ O_2 was the oxidizer.

The evidence presented above is generally consistent with the mechanism presented by Bachar and Rosenwaks [7] to account for the reaction between lead and $^1\Delta$ O_2. This mechanism is shown in the following reactions:

$$\mathrm{Pb}(^3\mathrm{P}_0) + \mathrm{O}_2(^1\Delta) \rightarrow \mathrm{Pb}(^3\mathrm{P}_1) + \mathrm{O}_2(^3\Sigma), \quad (16a)$$

$$\mathrm{Pb}(^3\mathrm{P}_1) + \mathrm{O}_2(^1\Delta) \rightarrow \mathrm{Pb}(^3\mathrm{P}_2) + \mathrm{O}_2(^3\Sigma), \quad (16b)$$

$$\mathrm{Pb}(^3\mathrm{P}_2) + \mathrm{O}_2(^1\Delta) \rightarrow \mathrm{PbO}(\mathrm{X}, v) + \mathrm{O}(^3\mathrm{P}), \quad (16c)$$

$$\mathrm{PbO}(\mathrm{X}, v) + \mathrm{O}_2(^1\Delta) \rightarrow \mathrm{PbO}(\mathrm{a}, \mathrm{b}) + \mathrm{O}_2(^3\Sigma), \quad (16d)$$

$$\mathrm{PbO}(\mathrm{a}, \mathrm{b}) + \mathrm{O}_2(^1\Delta) \rightarrow \mathrm{PbO}(\mathrm{A}, \mathrm{B}\ldots) + \mathrm{O}_3(^3\Sigma). \quad (16e)$$

The significant increase in intensity when $^1\Delta$ O_2 is the oxidizer indicates a significant change in mechanism to one in which the rate controlling step has a substantially lower activation energy. In the mechanism proposed by Bachar and Rosenwaks [7], the rate-controlling step in the sequence is the process shown in (16c), where PbO(X, v) indicates PbO in the vibrationally excited levels of the ground electronic state. This reaction is expected to have an activation energy much lower than that for the reactions shown in (14a) and (14b) or (15). The activation energy value for this reaction of 21.0 kcal/mol (see table 1) is substantially lower than those values obtained for the reaction with $^3\Sigma$ O_2. It was also observed that there is a slight decrease in activation energy with increasing crucible temperature. This decrease may indicate a change in mechanism for the reaction between Pb and $^1\Delta$ O_2 in which the vibrational level of PbO in (16c) is changing with changing temperature conditions in the reaction zone.

It can be pointed out that one additional step should be reasonably added to the Bachar–Rosenwaks mechanism. That step is the one involving the reaction between lead and the atomic oxygen formed as shown in (16c). This reaction is expected to be very fast and would not be evident in a kinetic analysis. However, based on the present work with $^3\Sigma$ O_2, it seems reasonable to include this reaction (14b) as a part of the mechanism. This step can at least partially account for the formation of the higher energy states since the reaction is exothermic enough to produce PbO* in the D and E states [4].

The observation that the change in relative intensities of chemiluminescence from different electronically excited states of PbO* with $^1\Delta$ O_2 pressure changes is less than the relative intensity changes where $^3\Sigma$ O_2 is the oxidizer provides further support for the modified Bachar–Rosenwaks mechanism. Since the rate-limiting reaction is fast it is relatively insensitive to whether Pb or Pb_2 is the reacting species. And since the energy transfer steps (16d) and (16e) are fast compared to (16c) then regardless of pressure the relative intensities of chemiluminescence will stay the same.

Based on the experimental evidence, there are significant differences in the mechanisms for the

Table 7
Franck–Condon factors for PbO a–X transitions

v'	v''																							
	0	1	2	3	4	5	6	7	8	9	10	11	12	13	14	15	16	17	18	19	20	21	22	23
0	005	033	091	160	202	195	149	092	045	018	006	002	000	000	000	000	000	000	000	000	000	000	000	000
1	025	096	151	114	028	003	065	139	156	118	065	028	010	003	001	000	000	000	000	000	000	000	000	000
2	060	138	093	005	033	097	065	004	028	107	144	117	067	029	010	003	000	000	000	000	000	000	000	000
3	101	121	013	033	085	024	010	076	067	006	024	101	136	108	060	025	002	000	000	000	000	000	000	000
4	133	064	008	079	023	016	071	023	010	074	056	002	034	108	130	095	018	005	001	000	000	000	000	000
5	146	014	053	048	005	064	016	020	064	011	021	076	038	000	054	120	078	035	012	003	001	000	000	000
6	139	001	076	004	049	029	012	057	004	035	053	001	040	071	017	010	128	106	058	023	007	001	000	000
7	118	020	055	010	054	000	052	009	029	042	001	052	032	003	060	053	035	109	125	084	038	013	003	001
8	092	051	020	044	018	030	029	012	045	000	046	018	015	056	008	023	026	004	071	126	108	059	022	006
9	066	076	001	057	000	049	000	045	005	034	021	013	046	001	039	039	052	057	003	031	107	125	082	036
10	045	086	007	040	019	027	019	027	012	034	004	043	001	037	023	009	011	020	068	025	005	075	127	105
11	029	082	030	014	043	002	042	001	039	002	036	007	027	023	009	044	037	037	001	053	052	001	039	114
12	018	070	054	000	045	006	031	013	024	014	025	010	031	003	039	001	021	010	051	007	025	060	017	012
13	011	054	069	007	026	029	006	035	001	035	000	035	001	034	005	027	011	040	000	041	029	004	059	041
14	006	038	071	028	006	041	002	030	010	021	016	016	017	018	013	026	036	000	039	013	018	047	001	038
15	003	025	064	049	000	032	019	009	030	001	032	000	031	001	032	000	001	032	011	020	032	002	047	016
16	002	015	051	061	012	013	035	000	029	009	017	018	010	022	008	023	020	016	013	029	003	041	003	031
17	001	009	037	063	031	001	033	012	010	027	000	029	001	026	004	024	026	003	031	000	035	002	032	019
18	000	005	024	056	049	004	018	029	000	027	009	013	019	005	025	002	001	028	002	028	005	025	016	014
19	000	002	015	045	058	019	003	032	009	010	025	000	026	003	020	009	013	013	015	015	013	020	008	030
20	000	001	009	033	057	037	001	020	024	000	025	009	010	020	002	025	025	001	025	002	027	001	030	000
21	000	000	005	022	050	050	011	006	029	006	010	023	000	023	005	015	007	020	004	023	002	025	003	026
22	000	000	002	013	039	055	027	000	021	020	000	023	008	008	020	000	001	020	006	016	010	014	012	015
23	000	000	001	008	028	051	042	006	008	027	005	010	021	000	020	007	017	002	022	000	023	001	024	002
24	000	000	000	004	018	043	050	020	000	021	017	000	021	008	006	020	020	005	013	012	007	018	003	022

Table 8
Franck–Condon factors for PbO A–X transitions

v'	v''																							
	0	1	2	3	4	5	6	7	8	9	10	11	12	13	14	15	16	17	18	19	20	21	22	23
0	026	097	179	218	197	141	082	039	015	005	001	000	000	000	000	000	000	000	000	000	000	000	000	000
1	091	180	127	022	009	083	148	149	104	054	022	007	002	000	000	000	000	000	000	000	000	000	000	000
2	165	129	004	051	108	049	000	048	122	139	101	053	021	007	002	000	000	000	000	000	000	000	000	000
3	204	028	046	095	011	029	090	047	000	048	119	129	088	044	017	005	000	000	000	000	000	000	000	000
4	190	003	102	013	040	074	005	035	082	030	003	065	123	116	072	032	003	001	000	000	000	000	000	000
5	143	058	058	020	074	001	051	052	000	053	070	011	016	089	125	099	020	006	001	000	000	000	000	000
6	090	116	003	077	011	043	044	004	062	025	010	069	046	000	044	112	076	034	011	003	000	000	000	000
7	049	131	017	061	015	058	001	058	012	026	057	003	036	069	016	010	124	099	051	018	005	001	000	000
8	024	108	070	010	064	006	049	019	024	046	000	052	029	005	063	046	046	115	117	070	028	008	002	000
9	010	072	106	006	056	016	044	009	049	000	050	013	022	005	002	035	012	016	093	125	089	040	012	003
10	004	041	105	047	012	058	002	051	004	042	014	024	039	001	051	022	065	035	001	065	125	107	054	018
11	002	020	080	087	003	050	019	030	021	029	013	039	002	047	007	028	000	047	056	002	037	115	120	069
12	001	009	051	098	036	012	054	000	048	000	044	000	043	005	031	028	052	010	023	065	015	016	099	130
13	000	004	028	081	075	002	043	024	017	033	010	032	013	024	025	009	000	041	028	006	062	033	003	079
14	000	001	013	055	090	032	009	052	001	039	008	031	009	033	004	039	041	011	022	044	000	048	049	000
15	000	000	006	032	079	068	003	035	031	006	039	000	039	000	038	001	008	025	028	006	049	006	030	060
16	000	000	002	016	056	084	031	005	048	007	026	021	013	026	010	025	020	024	009	040	000	044	019	014
17	000	000	001	007	033	075	064	004	026	037	001	038	003	030	007	027	029	005	036	000	041	005	031	033
18	000	000	000	003	017	054	078	033	002	043	015	014	031	002	034	000	000	035	000	036	003	032	016	016
19	000	000	000	001	008	033	070	062	007	018	040	001	030	013	015	022	027	006	028	007	026	014	018	029
20	000	000	000	000	003	018	051	073	035	000	036	023	004	034	001	028	021	012	018	014	019	012	026	007
21	000	000	000	000	001	008	032	065	061	011	011	040	005	019	024	003	000	030	002	028	003	029	003	033
22	000	000	000	000	001	008	032	065	061	011	011	040	005	019	024	003	000	030	002	028	003	029	003	033
23	000	000	000	000	000	001	008	029	060	060	016	005	037	012	009	029	026	008	016	017	009	023	005	026
24	000	000	000	000	000	001	004	016	043	065	042	002	020	034	001	022	004	028	000	025	006	019	012	015

Table 9
Franck–Condon factors for PbO B–X transitions

v'	v''																							
	0	1	2	3	4	5	6	7	8	9	10	11	12	13	14	15	16	17	18	19	20	21	22	23
0	049	160	244	235	165	090	039	014	004	001	000	000	000	000	000	000	000	000	000	000	000	000	000	000
1	126	196	073	001	079	166	168	112	053	019	005	001	000	000	000	000	000	000	000	000	000	000	000	000
2	176	090	006	112	086	003	045	139	159	109	051	018	005	001	000	000	000	000	000	000	000	000	000	000
3	178	009	085	069	003	090	074	002	047	136	148	095	043	015	004	001	000	000	000	000	000	000	000	000
4	150	008	101	000	080	044	009	089	054	000	065	140	133	079	033	011	000	000	000	000	000	000	000	000
5	111	045	049	037	063	005	080	018	028	089	029	008	090	142	115	061	007	001	000	000	000	000	000	000
6	076	075	007	079	005	064	024	028	068	001	056	075	007	030	115	137	042	014	003	001	000	000	000	000
7	049	084	002	067	014	059	007	066	001	059	037	008	077	046	001	065	123	068	026	007	001	000	000	000
8	030	076	019	031	052	012	054	014	040	036	012	067	006	036	077	015	105	139	098	044	014	003	000	000
9	018	061	035	006	064	002	058	006	054	002	060	004	046	043	002	067	000	059	135	125	068	025	006	001
10	011	046	043	000	049	026	022	045	011	043	016	031	039	007	062	010	077	016	018	107	142	096	041	012
11	007	033	043	005	026	046	001	057	004	047	005	049	001	056	006	039	001	066	051	000	064	141	122	063
12	004	023	039	012	009	048	006	035	033	013	041	008	038	017	028	038	059	011	030	075	012	023	118	143
13	003	017	032	016	002	039	020	010	051	001	046	007	039	005	046	001	005	038	041	002	069	043	002	081
14	002	012	026	018	000	026	030	000	044	018	019	037	006	039	006	038	029	033	007	058	007	038	070	006
15	001	009	021	018	001	015	033	002	026	037	001	047	005	035	009	034	043	002	050	002	042	034	008	073
16	001	006	017	017	002	008	029	009	010	043	005	029	029	008	037	003	004	041	009	034	025	013	056	001
17	001	005	013	015	004	003	023	014	002	035	018	008	044	001	036	009	012	029	012	036	006	045	000	051
18	001	004	011	013	005	001	017	017	000	024	029	000	038	018	013	034	036	001	040	000	044	002	039	015
19	000	003	009	012	005	000	012	017	001	013	031	003	022	035	000	038	024	014	019	020	020	022	024	014
20	000	002	007	010	005	000	009	015	003	006	028	010	008	039	005	022	003	034	000	035	001	039	001	041
21	000	002	006	009	005	000	006	013	005	002	022	016	001	032	018	006	003	026	014	014	022	010	030	008
22	000	002	005	007	005	000	004	011	006	000	015	018	000	021	028	000	019	007	032	000	030	002	031	007
23	000	001	004	006	004	000	003	009	006	000	010	018	002	011	030	004	033	000	029	012	013	022	005	031
24	000	001	004	005	004	000	002	007	006	000	007	016	005	005	027	011	035	008	014	029	000	028	003	024

Table 10
Franck–Condon factors for PbO A–a transitions

v'	v''																							
	0	1	2	3	4	5	6	7	8	9	10	11	12	13	14	15	16	17	18	19	20	21	22	23
0	918	070	010	002	000	000	000	000	000	000	000	000	000	000	000	000	000	000	000	000	000	000	000	000
1	082	765	120	026	006	001	000	000	000	000	000	000	000	000	000	000	000	000	000	000	000	000	000	000
2	000	164	623	154	043	012	003	001	000	000	000	000	000	000	000	000	000	000	000	000	000	000	000	000
3	000	000	244	493	174	060	020	006	002	000	000	000	000	000	000	000	000	000	000	000	000	000	000	000
4	000	000	002	320	378	182	075	029	010	003	001	000	000	000	000	000	000	000	000	000	000	000	000	000
5	000	000	000	004	390	277	180	086	038	015	005	002	001	000	000	000	000	000	000	000	000	000	000	000
6	000	000	000	000	009	451	193	171	094	048	021	008	003	001	000	000	000	000	000	000	000	000	000	000
7	000	000	000	000	001	016	502	125	157	098	056	027	012	005	002	001	000	000	000	000	000	000	000	000
8	000	000	000	000	000	001	026	541	071	140	099	063	033	016	007	002	000	000	000	000	000	000	000	000
9	000	000	000	000	000	000	001	041	567	033	122	097	068	039	020	009	001	000	000	000	000	000	000	000
10	000	000	000	000	000	000	000	000	061	576	010	103	093	071	045	024	004	002	001	000	000	000	000	000
11	000	000	000	000	000	000	000	000	000	087	567	000	085	088	073	050	013	006	002	001	000	000	000	000
12	000	000	000	000	000	000	000	000	000	000	118	542	004	067	082	073	032	016	007	003	001	000	000	000
13	000	000	000	000	000	000	000	000	000	001	000	155	501	018	051	076	057	036	019	009	004	001	000	000
14	000	000	000	000	000	000	000	000	000	000	001	002	194	447	042	035	070	059	040	023	011	005	002	001
15	000	000	000	000	000	000	000	000	000	000	000	001	004	235	382	073	061	067	060	044	026	014	006	002
16	000	000	000	000	000	000	000	000	000	000	000	000	002	009	274	311	010	054	063	061	047	030	016	008
17	000	000	000	000	000	000	000	000	000	000	000	000	000	003	017	309	148	003	045	060	060	050	033	019
18	000	000	000	000	000	000	000	000	000	000	000	000	000	001	005	028	166	184	000	037	056	059	052	037
19	000	000	000	000	000	000	000	000	000	000	000	000	000	000	001	008	353	101	214	003	029	051	057	053
20	000	000	000	000	000	000	000	000	000	000	000	000	000	000	000	002	061	356	048	234	014	020	047	055
21	000	000	000	000	000	000	000	000	000	000	000	000	000	000	000	000	018	081	343	014	240	031	012	043
22	000	000	000	000	000	000	000	000	000	000	000	000	000	000	000	000	005	026	104	314	000	230	055	005
23	000	000	000	000	000	000	000	000	000	000	000	000	000	000	000	000	000	008	037	125	270	008	204	084
24	000	000	000	000	000	000	000	000	000	000	000	000	000	000	000	000	000	001	012	051	143	215	035	164

formation of PbO. These differences are related to the electronic state of the oxidizer. The faster rate and greater intensity of emissions observed when $^1\Delta$ O_2 is the oxidizer indicate that the rate-controlling step (i.e. the step in which O–O bond must be broken) is much more probable if the oxygen and the Pb are in higher energy states. On the other hand, when $^3\Sigma$ O_2 is the oxidizer, there are no fast preliminary reactions which can operate to prepare the system for the relatively fast rate-controlling step. Under these conditions it is reasonable to postulate that the formation of PbO* is due to one of two mechanisms. The first involves the formation of atomic oxygen in a very slow, endothermic, or possibly slightly exothermic, reaction followed by a fast reaction between Pb and the oxygen atom. The second mechanism involves the exothermic reaction between molecular oxygen and Pb_2 in a four-center-type reaction to produce one molecule of ground state PbO and one molecule of electronically excited PbO*.

Acknowledgement

This research was supported in part by a grant from the Air Force Office of Scientific Research under grant number AFOSR/AFIT 83-1. The authors would like to thank Mr. Curtis Atnipp for technical support given during the course of this project.

Appendix

A listing of selected Franck–Condon factors is given in tables 7–10. (Values in the tables are FC factor $\times 1000$.)

References

[1] S. Bloomenthal, Phys. Rev. 35 (1930) 34.
[2] R.C. Oldenborg, C.R. Dickson and R.N. Zare, J. Mol. Spectry. 58 (1975) 238.
[3] M.J. Kurylo, W. Braun, S. Abramowitz and M. Krauss, J. Res. Nat. Bur. Std. 80A (1976) 167.
[4] C. Linton and H.P. Broida, J. Mol. Spectry. 62 (1976) 396.
[5] J.M. Brom Jr. and W.H. Beattie, J. Mol. Spectry. 81 (1980) 445.
[6] B.G. Wicke, S.P. Tang and J.F. Friichtenicht, Chem. Phys. Letters 53 (1978) 304.
[7] S. Bachar and S. Rosenwaks, Chem. Phys. Letters 96 (1983) 526.
[8] E.A. Dorko, J.W. Glessner, C.M. Ritchey and S.R. Snyder, Chem. Phys Letters 109 (1984) 18.
[9] B. McCarroll, Rev. Sci. Instr. 41 (1970) 219.
[10] K. Furukawa and E.A. Ogryzlo, Chem. Phys. Letters 12 (1971) 370.
[11] S.I. Steinfeld, Molecules and radiation (MIT Press, Cambridge, MA, 1978).
[12] S. Mrozowski, Phys. Rev. 34 (1940) 1086.
[13] E.U. Condon and G.H. Shortley, The theory of atomic spectra (Cambridge University Press London, 1963).
[14] R.H. Garstang, J. Res. Nat. Bur. Std. 68A (1964) 61.
[15] D. Husain and J.G.F. Littler, Intern. J. Chem. Kinetics 6 (1974) 61.
[16] W.F. Meggers and F.O. Westfall, J. Res. Natl. Bur. Std. (1950) 447.
[17] D.R. Wood and K.L. Andrew, J. Opt. Soc. Am. 58 (1968) 818.
[18] C.E. Moore, Atomic energy levels, NBS Circular 467 (Natl. Bur. Std., Washington, 1949).
[19] J.P. Duray, Spectroscopic Studies of Lead Oxide in a Flow Tube, M.S. Thesis, Air Force Institute of Technology, Wright–Patterson AFB, Ohio, USA (December, 1984).
[20] L.D. Brasure, Calculation of Franck–Condon Factors for Diatomic Molecules, M.S. Thesis, Air Force Institute of Technology, Wright–Patterson AFB, Ohio, USA (March, 1985).
[21] H. Scheingraber and C.R. Vidal, J. Mol. Spectry. 65 (1977) 46.
[22] C.R. Vidal, J. Chem. Phys. 72 (1980) 1864.
[23] W.C. Stawalley and C.R. Vidal, J. Chem. Phys. 77 (1982) 883.
[24] R. Rydberg, Z. Physik 73 (1932) 376.
[25] O. Klein, Z. Physik 76 (1932) 226.
[26] A.L.G. Rees, Proc. Phys. Soc. (London) 59 (1947) 98.
[27] J. Hinze and M.K. Kosman, J. Mol. Spectry. 56 (1975) 93.
[28] C.M. Ritchey, Spectroscopy and Kinetics of Lead Oxide Chemiluminescence, M.S. Thesis, Air Force Institute of Technology, Wright–Patterson AFB, Ohio, USA (December, 1983).
[29] B. Rosen, Spectroscopic data relative to diatomic molecules (Pergamon Press, New York, 1970).
[30] R.F. Barrow, J.L. Deutsch and D.H. Travis, Nature 191 (1961) 374.
[31] K.P. Huber and G. Herzberg, Molecular spectra and molecular structure, Vol. 4. Constants of diatomic molecules (Van Nostrand–Reinhold, New York, 1979).
[32] J. Tellinghuisen, J. Mol. Spectry. 103 (1984) 455.
[33] S.N. Suchard, Spectroscopic data for heteronuclear diatomic molecules, Vol. 2 (Plenum Press, New York, 1975).
[34] S.E. Johnson, Spectroscopy of Selected Diatomic Metal and Metal Oxide Molecules Using Laser Excited Fluorescence, PhD. Dissertation, University of California, Santa Barbara, California, USA (December, 1971).